Supporting Information

Exploration of the synergistic regulatory mechanism of hydroxide and fluoride modification on the photocatalytic activity of 2D g-C_3N_4

Qianqian Shang[1], Hongbing Wang[2], Changjie Kan[1], Rui Ding[2], Yankai Li[2], Shiva Pandeya[2,3], Ziliang Li[2]*, Mahesh Kumar Joshi[2,3]*

[1]School of Chemistry and Chemical Engineering, Liaocheng University, Liaocheng 252059, China.
[2]School of Materials Science and Engineering, Liaocheng University, Liaocheng 252059, China. [3]Central Department of Chemistry, Tribhuvan University, Kirtipur, Kathmandu, Nepal

Email: mahesh.joshi@trc.tu.edu.np, sdlizl1986@163.com

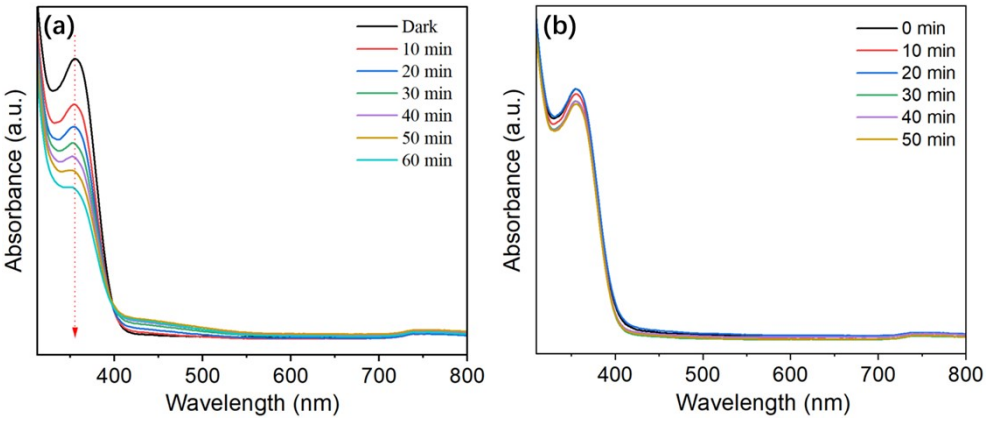

Figure S1. The UV-Vis absorbance spectra of the tetracycline (TC, 20 mg/L) degradation under light illumination (a) with and (b) without HF-CNS as photocatalyst for different time.

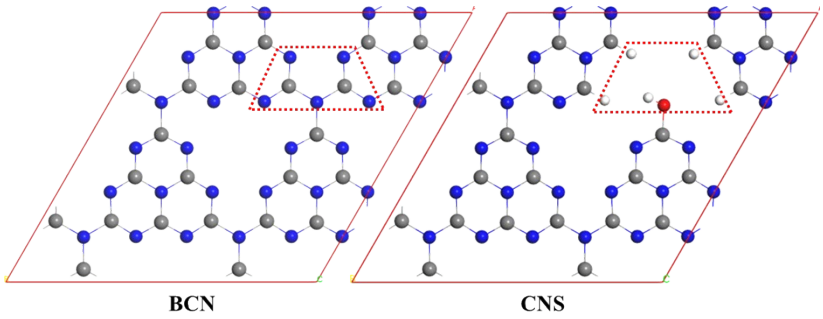

Figure S2. The initial configuration of BCN and CNS.

Surface area and pore size distribution

Nitrogen adsorption-desorption measurements were performed to investigate the BET (Brunauer-Emmett-Teller) surface area and pore size distribution of different samples. It can be clearly seen in Figure S2 that all samples exhibit type V isotherms with H_3 hysteresis loops in the high relative pressure range between 0.5 and 1.0, suggesting that all the samples have mesoporous structure (1). Based on the N_2 adsorption-desorption curves, the BCN shows the lowest BET surface area (18.65 m^2/g). However, after ethanol-thermal treatment and fluorine assisted ethanal treatment, the BET specific surface area of BCN was increased to 128.03 m^2/g and 159.87 m^2/g, respectively, indicating that the ethanol-thermal treatment could effectively improve the surface area of g-C_3N_4, especially after the HF acid assisted ethanol-thermal treatment. This tendency is consistent with the above results of SEM and HR-TEM images, supporting the morphologic structure variation of BCN, CNS and HF-CNS.

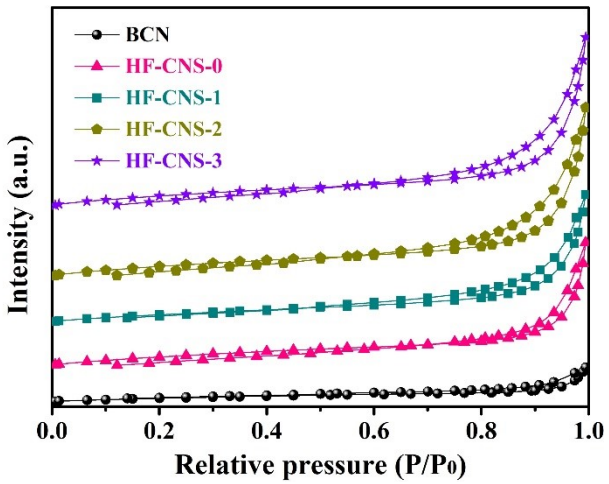

Figure S3. N_2 adsorption-desorption isotherm curves of the BCN, HF-CNS-0, HF-CNS-1, HF-CNS-2 and HF-CNS-3 measured at 77 K by the Brunauer-Emmett-Teller (BET) method.

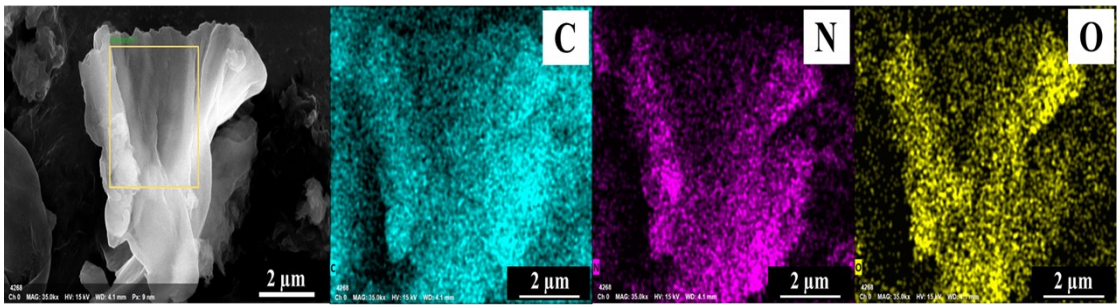

Figure S4. SEM-EDS elemental mappings of the CNS.

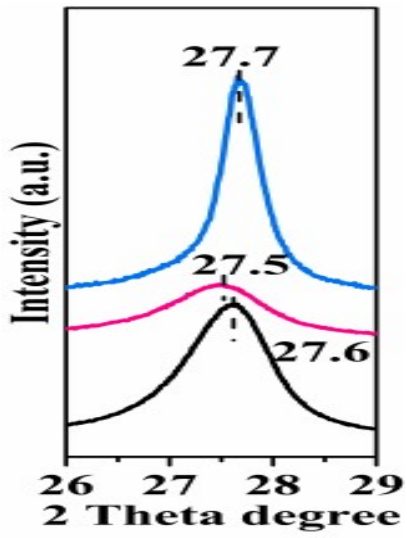

Figure S5. The magnified XRD patterns of BCN, CNS and HF-CNS-2 from 26° to 29°.

Table S1. The element composition of as-prepared catalysts (C, N, O, F atomic %) for BCN, CNS and F-CNS calculated from the XPS survey spectra.

	C	N	O	F	C/N	
BCN	42.6	56.52	0.88	0	3/3.98	0.75
CNS	40.35	56.98	2.67	0	3/4.23	0.71
HF-CNS-2	43.08	52.11	3.99	0.81	3/3.56	0.84

Table S2. The content ratio of function groups in the samples obtained in the high-resolution C 1s spectra.

	C-OH	N-C=N
BCN	1.30	19.62
CNS	6.25	14.51
HF-CNS-2	5.65	14.34

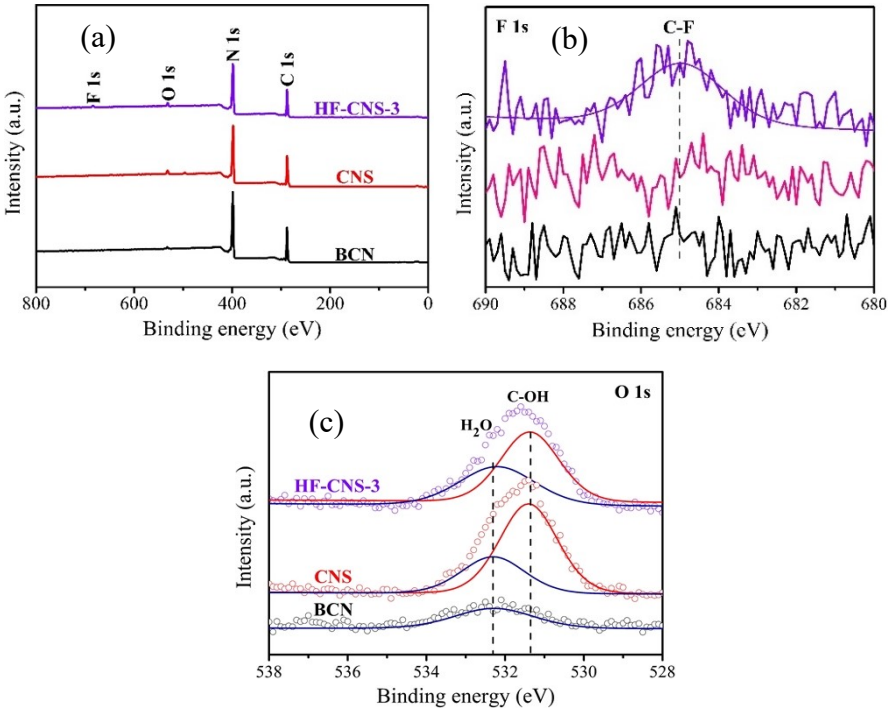

Figure S6. The XPS survey scan (a) and the high-resolution XPS of (b) F 1s and (c) O 1s spectra of BCN, CNS and F-CNS-2.

Table S3. The content ratio of function groups in the samples obtained in the high-resolution N 1s spectra.

	C-N=C	**N-$(C)_3$**	**C-N-H**	**π-excitations**
BCN	58.67	23.28	7.82	10.22
CNS	61	21.47	6.09	11.45
HF-CNS-2	51.34	30.2	10.77	7.68

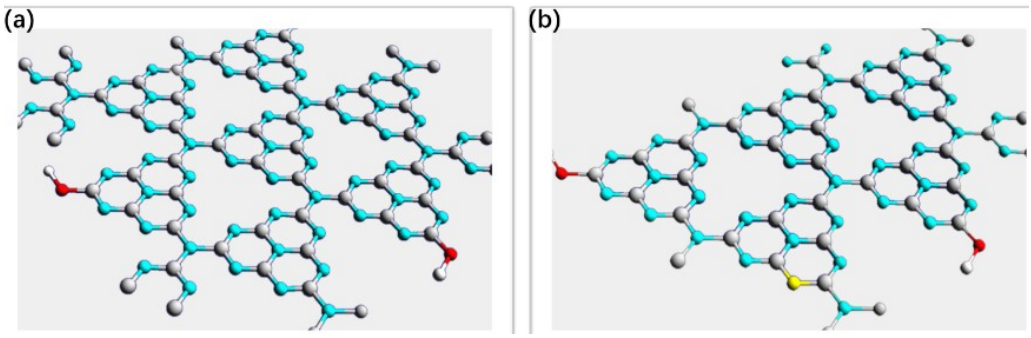

Figure S7. (a) The possible types of HF-CNS in the red dashed cycles, (b) possible types of HF-CNS-3 are shown in the red dashed cycles.

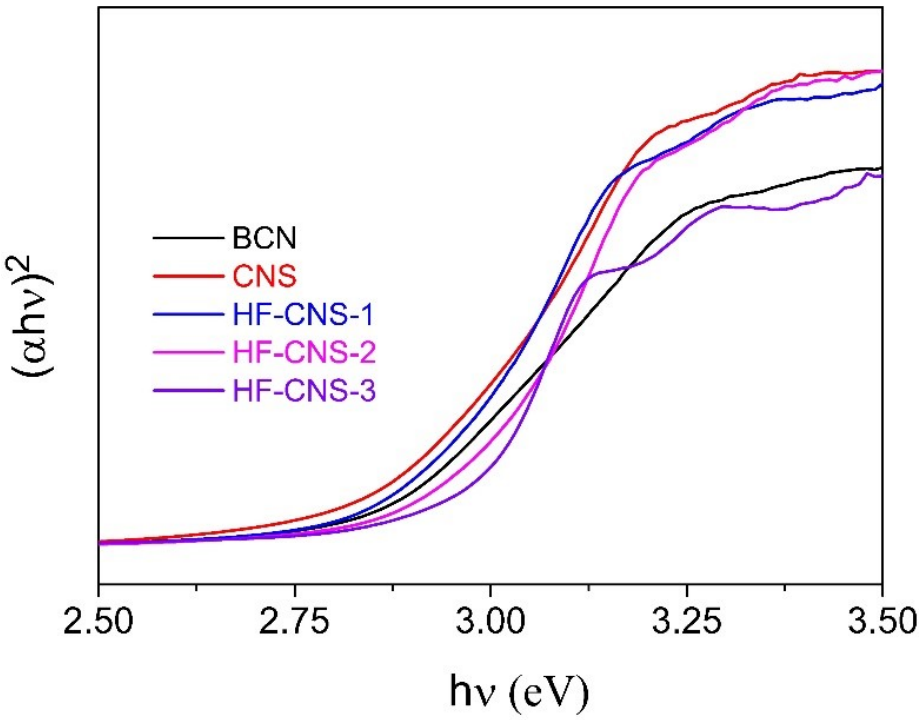

Figure S8. The band energy of the BCN, CNS and HF-CNS-X (X=1, 2, 3).

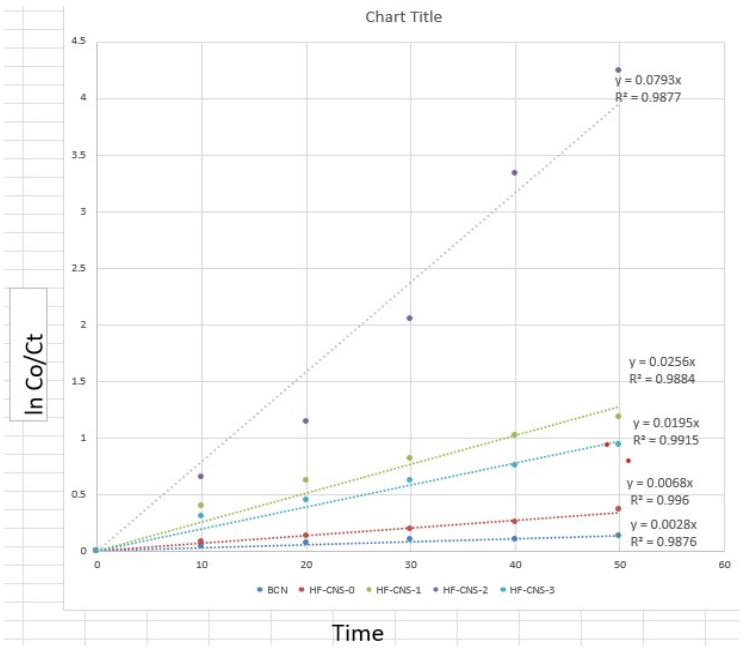

Figure S9. Pseudo-first-order curve fitting for different samples.

Table S4. A comparison of g-C_3N_4 prepared from different precursors as photocatalysts.

Carbon nitride	Precursors	Application	Activity	Ref.
Polymeric C_3N_4	Dicyandiamide; 5-bromo-2-thiophenecarboxaldehyde; NH_4Cl	H_2 production	2.448 mmol g^{-1} h^{-1}	(2)
F-doped g-C_3N_4	melamine	H_2 production	6 μmol g^{-1} h^{-1}	(3)
g-C_3N_4	soaking melamine in aqueous solutions	H_2 production	1.82 μmol g^{-1} h^{-1}	(4)
F-doped g-C_3N_4	urea	Photodegradation of Rhodamine B	0.02 min^{-1}	(1)
Chloride-modified g-C_3N_4	urea	CO_2 reduction	14 μmol g^{-1} h^{-1}	(5)
F-doped g-C_3N_4	melamine	H_2 production	1.1 mmol h^{-1}	this work
F-doped g-C_3N_4	melamine	TC degradation	0.0079 min^{-1}	this work

References

1. Bai X, Wang X, Lu X, Jia T, Sun B, Wang C, et al. A fluorine induced enhancement of the surface polarization and crystallization of g-C_3N_4 for an efficient charge separation. New Journal of Chemistry. 2021;45(21):9334-45.

2. Liu R, Liu S, Lin J, Li Y, Chen S, Wang P, et al. Donor-acceptor anchoring nanoarchitectonics in polymeric carbon nitride for rapid charge transfer and enhanced visible-light photocatalytic hydrogen evolution reaction. Carbon. 2022;197:378-88.

3. Zeng L, Ding X, Sun Z, Hua W, Song W, Liu S, et al. Enhancement of photocatalytic hydrogen evolution activity of g-C_3N_4 induced by structural distortion via post-fluorination treatment. Applied Catalysis B: Environmental. 2018;227:276-84.

4. Barrio J, Grafmüller A, Tzadikov J, Shalom M. Halogen-hydrogen bonds: A general synthetic approach for highly photoactive carbon nitride with tunable properties. Applied Catalysis B: Environmental. 2018;237:681-8.

5. Li J, Zhang X, Raziq F, Wang J, Liu C, Liu Y, et al. Improved photocatalytic activities of g-C_3N_4 nanosheets by effectively trapping holes with halogen-induced surface polarization and 2, 4-dichlorophenol decomposition mechanism. Applied Catalysis B: Environmental. 2017;218:60-7.